

Article

Variable Switching Frequency for ZVS over Wide Voltage Range in Dual Active Bridge

Alberto Cárcamo ^{1,*}, Alejandro Fernandez-Hernandez ², Fernando Gonzalez-Hernando ², Aitor Vázquez ¹
and Alberto Rodríguez ¹

¹ Electrical, Electronic, Communications and Systems Engineering Department, Universidad de Oviedo, 33204 Gijón, Spain; vazquezaitor@uniovi.es (A.V.); rodriguezalberto@uniovi.es (A.R.)

² Ikerlan Technology Research Centre, Basque Research and Technology Alliance (BRTA), P° J.M. Arizmendiarieta, 2., 20500 Arrasate/Mondragón, Spain; alejandro.fernandez@ikerlan.es (A.F.-H.); fgonzalez@ikerlan.es (F.G.-H.)

* Correspondence: carcamoalberto@uniovi.es

Abstract: The Dual Active Bridge (DAB) converter is known for its advantageous characteristics, including bidirectionality, galvanic isolation, and soft-switching operation. However, achieving Zero Voltage Switching (ZVS) across the complete operation range is not guaranteed, particularly through a wide input–output voltage ratio. This paper explores the integration of the switching frequency as a control variable in the DAB converter to ensure ZVS operation across a wide voltage range, employing Single Phase Shift (SPS) modulation. The study evaluated the RMS and reactive currents under variable switching frequency, presenting the advantages of this approach. Moreover, it includes a design-oriented analysis of the ZVS limits and their relationship with the switching frequency, aiming to ensure ZVS at any operating point. Experimental results validated the theoretical analysis, while presenting the main advantages of variable switching frequency implementation.

Keywords: dual active bridge; frequency modulation; soft-switching; zero-voltage switching



Citation: Cárcamo, A.; Fernandez-Hernandez, A.; Gonzalez-Hernando, F.; Vázquez, A.; Rodríguez, A. Variable Switching Frequency for ZVS over Wide Voltage Range in Dual Active Bridge. *Electronics* **2024**, *13*, 1800. <https://doi.org/10.3390/electronics13101800>

Academic Editors: Jizhong Zhu, Yun Liu, Lei Xi and Weiye Zheng

Received: 18 April 2024

Revised: 2 May 2024

Accepted: 6 May 2024

Published: 7 May 2024



Copyright: © 2024 by the authors. Licensee MDPI, Basel, Switzerland. This article is an open access article distributed under the terms and conditions of the Creative Commons Attribution (CC BY) license (<https://creativecommons.org/licenses/by/4.0/>).

1. Introduction

The Dual Active Bridge (DAB) converter is widely utilized for several applications, including grid power transmission and automotive applications. Despite having been studied for several decades [1–6], the DAB converter remains popular today and is extensively employed in diverse applications, including battery chargers for electric vehicles. It offers several attractive characteristics, including bidirectional power transfer, galvanic isolation, high power density, and soft-switching capability.

The DAB converter consists of two Full Bridges (FB) connected through an inductor and a transformer that provides galvanic isolation. Its electrical schematic is described in Figure 1, where the sum of inductor and the transformer leakage inductance is represented by L_k , V_1 and V_2 are the input and output DC voltages, respectively, and v_1 and v_2 are the AC voltages at their respective FB. In this analysis, Single Phase Shift (SPS) modulation is utilized, which is widely employed in industry due to its simplicity and ease of implementation. It consists in controlling the power flow with a phase shift between both FBs, and it is further discussed in the next section.

There have been numerous studies with the objective of expanding the soft-switching operation range of the DAB converter. Among these studies, several modulation strategies have been proposed using the Pulse Width Modulations (PWMs) of the FBs as an additional control variable. One such strategy is the Double Phase Shift (DPS) modulation [7], which consists in varying the phase shift between the branches of one FB, as well as the phase shift between both FBs. Additionally, it is possible to vary the phase shift of the branches in both FBs, along with the phase shift between the FBs, adding additional degrees of freedom and resulting in more complex modulation known in some literature as Triple Phase Shift

(TPS) [8,9]. Some studies combine all the previously mentioned modulation techniques along an operation profile [10,11]. Also, these techniques may be employed to optimize the performance of the converter, e.g., for minimizing conduction losses [12]. All of these are modulation methods which can be easily adapted to any design of the converter and any change in the operating point. One of the main drawbacks is the increased complexity in the implementation.

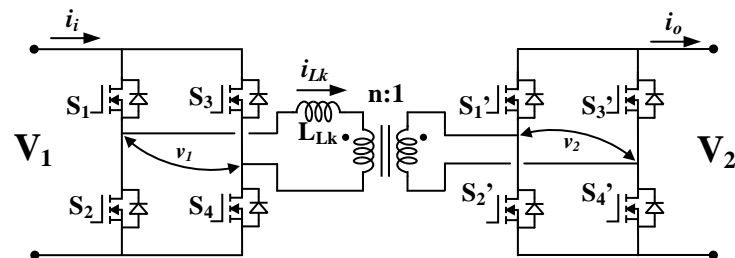


Figure 1. DAB converter electrical schematic.

Besides modulation strategies for the DAB converter and soft switching may also be extended by hardware methods. Some literature includes the use of the transformer magnetizing current to provide the energy for the parasitic capacitances. Others consider using several inductors controlled through additional switches to modify the inductance [13], or directly modify the inductance value using a variable inductor [14]. These solutions have some drawbacks including the need for additional components or the adaptability of the design to work in other operating conditions.

The control strategies based on varying the switching frequency in DAB can be classified into three categories [6]: those which employ the switching frequency as a control variable for regulating the power; those which adopt the switching frequency for extending the maximum power of DAB; and those which use the switching frequency for expanding the soft-switching operational range. All of them share its relative simplicity as the main benefit. In all the cases, the resulting control law is a linear relationship, which is advantageous compared to phase-shift modulations. However, there are some limitations to highlight. These techniques have in common the main disadvantages already reported when the control varies the frequency: increase in the current harmonic content (and therefore, more complex design of EMI filters which leads to bulkier stages); more complex design in general for estimating the power loss (and hence, for getting an optimum design); and practical limitations in the frequency range (the lowest frequency is limited by the audible frequency, i.e., 8 kHz, and the highest frequency is restricted by the switching characteristics of the power transistor technology used).

In the case of those solutions which use the switching frequency for extending the soft-switching operational range, there have been several studies with different approaches applied to the DAB. In [15], variable frequency is employed for the DAB converter operating at a fixed input–output voltage ratio. It calculates the optimum switching frequency for different output power based on a power loss model. In [16], variable frequency is used to improve the efficiency at light loads, although it is used in combination with a particular transformer, denominated dual leakage transformer. In [17], switching frequency is used in a control algorithm to increase power range and extend Zero-Voltage Switching (ZVS). It consists of using two switching frequencies, the lower frequency to increase the power of the converter, and at the higher frequency to maintain ZVS at low power. In [18], an optimal, full-operating-range ZVS modulation scheme is presented, which includes variable frequency, although the DAB converter is part of a two-stage ac–dc converter. In [19], variable frequency is employed in SPS modulation, at low power to keep the converter working with ZCS. A power loss analysis is performed using variable frequency and compared to constant frequency. In [20], a modulation strategy which includes variable frequency is presented. It considers three modulation strategies, for low-, medium-, and high-power levels, oriented to minimize conduction losses. The switching frequency varies

at medium power, transitioning from maximum frequency at low power, to minimum frequency at high power. In [21] a variable frequency control is presented which includes a Maximum Power Point Tracking (MPPT) using the perturb and observe technique to minimize the RMS currents. It develops a generalized state space average model to obtain a new small-signal model between the switching frequency and the output voltage. In [22], a Variable Frequency Modulation (VFM) is presented, with a closed-form algorithm to allow the converter to operate with ZVS over a wide power range with minimum reactive currents. It discusses the phase drift phenomenon, presenting a compensation scheme to ensure the operation of the VFM. In [23], an optimization technique is presented, where the converter works at an optimal constant phase shift, defined by the voltage ratio, to obtain minimum RMS currents. It proposes varying the switching frequency to modulate the power. In [24], a full ZVS control is proposed for a single-stage semi-DAB ac–dc converter, in which variable frequency control is implemented to extend ZVS operation. In [25], The primary side works at half the switching frequency of the secondary side using a modulation method denominated in the article as asymmetric half-frequency modulation (AHFM). In [26], the EMI in the DAB converter using variable switching frequency modulation (VSFM) is analyzed, and an improved VSFM is proposed. There are studies that combine variable frequency with modulation techniques such as Extended Phase Shift (EPS) [27–29].

As the main contribution, this paper presents a design-oriented analysis of the DAB converter, with the aim of ensuring ZVS operation in any operating point over a wide voltage range. This is done by including the switching frequency as a control variable. Moreover, it presents the behavior of the RMS and the reactive currents analyzed at constant power and variable switching frequency. Analyzing the converter at a constant power operation facilitates the understanding of working with variable switching frequency, emphasizing the dependence between the input–output voltage ratio and the phase-shift angle. This is a general analysis that can be applied to any operating point and extended to any application. This paper is organized as follows: In Section 2, a brief description of the operation principles of the DAB converter is presented. In Section 3, the RMS and reactive currents are discussed, along with the ZVS limits. The experimental results are discussed in Section 4, and the conclusions are presented in Section 5.

2. DAB Converter Operating Principles

One of the main advantages of this topology is its ability to achieve soft-switching operation, either with ZVS or Zero Current Switching (ZCS). ZVS is achieved using reactive currents, which enable a soft turn-on of the MOSFETs during the dead time interval. ZCS can be achieved by implementing modulation methods (DPS, TPS, etc.), that allow the converter to switch the devices when the inductor current is zero. It is well known that ZVS is not guaranteed for every operating point, as it depends mainly on the power managed and on the input–output voltage ratio, $M = \frac{nV_2}{V_1}$. Note that the definition of M in this paper is the voltage ratio, regardless of the power transfer direction and is not to be confused with the converter gain.

The power flow in the DAB converter has been widely studied and it depends on several parameters, some of which can be used as control variables. The average power flow using SPS can be described by the following:

$$P = \frac{V_1 V_2 n \varphi (\pi - \varphi)}{2\pi^2 f_s L_k} \quad (1)$$

where V_1 , V_2 , and L_k , can be considered as constant for a given operating point, leaving the switching frequency, f_s , and the phase shift, φ , as the control variables. It could be possible to control the voltages, e.g., by adding additional converters stages connected through a dc-link. The inductor can also become a control variable, either by using more than one inductor connected through switches [13], or by using a variable inductor [14], as is exposed in the previous section.

The simplest modulation method is the SPS, which consists of controlling the power transfer by modifying the phase shift between both FBs, while their PWMs are kept constant at a duty cycle of 50%. This modulation technique has several advantages, such as its simplicity, low computational demand, and its capability to achieve full power, while other modulation methods limit the converter maximum power. In Figure 2, the SPS modulation waveforms are presented considering a positive power transfer, from FB₁ to FB₂. The phase-shift angle, φ , between v_1 and v_2 , generates the inductor current i_{Lk} . The current value at the switching instants of FB₁ and FB₂ power devices, i_1 and i_2 , respectively, are shown in the figure and can be defined as follows:

$$i_1 = \frac{1}{4\pi f_s L_k} (V_1\pi + V_2n(2\varphi - \pi)) \tag{2}$$

$$i_2 = \frac{1}{4\pi f_s L_k} (V_1(2\varphi - \pi) + V_2n\pi). \tag{3}$$

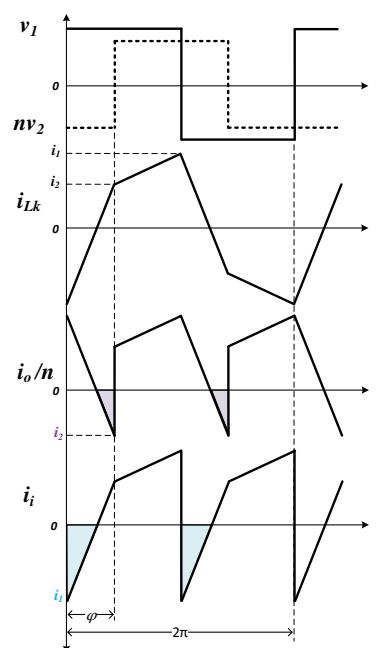


Figure 2. The converter waveforms from top to bottom: voltages V_1 and V_2 , the current through the inductor, i_{Lk} , the input current, i_i , and the output current, i_o . The waveforms are referred to as FB₁.

The output and input current waveforms, i_o and i_i , respectively, are shown in Figure 2, where the shaded area represents the reactive currents, with its value at the switching instant of the corresponding FB shown in its respective color. The reactive currents are discussed in the next section.

This modulation technique achieves the maximum power transfer at a phase-shift angle of $\frac{\pi}{2}$, although a lower phase-shift angle is usually chosen for achieving the maximum rated power at the design stage of the converter. This is due to the loss of linearity around angles greater than $\frac{\pi}{3}$, making it harder to control, as well as a lower increment in the power transfer with respect to the phase shift. It is also important to note that this modulation has high reactive currents, and the fact that they increase with the phase-shift angle implies that lower phase-shift angles are to be preferred, as it benefits the converter regarding conduction losses. However, as it is explained in the next section, for operating points where $M \neq 1$, there is a minimum phase shift that limits the ZVS operation of the converter.

3. Variable Switching Frequency

3.1. RMS and Reactive Currents

ZVS operation in the DAB converter working with SPS modulation depends on the inductor current at a switching instant being high enough to charge/discharge the parasitic capacitances on the MOSFETs. The inductor current value at the switching instants, i_1 and i_2 from Figure 2, must be positive to guarantee ZVS in its respective FB. These current values are also shown for the output and input currents in the last two waveforms from top to bottom. These are the reactive currents that flow through the body diode of the MOSFET during the dead time, allowing ZVS operation in their respective FBs.

The RMS current through the inductor, $i_{Lk_{RMS}}$, can be calculated using (2) and (3) and is defined as [30]:

$$i_{Lk_{RMS}} = \sqrt{\left(\frac{(\varphi)(i_1^2 + i_2^2 - i_1 i_2) + (\pi - \varphi)(i_1^2 + i_2^2 + i_1 i_2)}{3\pi} \right)}. \quad (4)$$

Considering a constant power operation, it is possible to vary the switching frequency as a function of the phase shift and obtain $i_{Lk_{RMS}}$. Figure 3 shows the normalized $i_{Lk_{RMS}}$ for different values of M , as a function of the phase shift and the normalized switching frequency, with the latter shown in red and referred to the right y-axis. The dashed lines represent the ZVS limit for each case in their corresponding color. These ZVS limits are obtained using (8). The figures presented in this paper are generated using Matlab R2022b. Note that as the phase shift tends to zero, so does the switching frequency. Therefore, it is important to define a minimum switching frequency, which is limited by the magnetic devices, as low frequencies may increase the magnetic flux density in the core, causing high power losses and potentially the saturation of the core. The currents are normalized with respect to the average input current, given by the power and the input voltage for each value of M , and can be described as follows:

$$i_{Lk_{RMS}}[pu] = \frac{i_{Lk_{RMS}}}{\frac{P}{V_1}}. \quad (5)$$

The switching frequency is normalized with respect to the maximum switching frequency for each value of M , and can be described as follows:

$$f_s[pu] = \frac{f_s}{f_{smax}}, \quad (6)$$

where f_{smax} is the switching frequency at the maximum phase shift for a constant power operation. The minimum $i_{Lk_{RMS}}$ is marked with an 'x' for each curve in their respective colors. The figure shows that for $M = 1$, the RMS current always increases with the phase shift, and the lowest value is at the lowest possible phase shift. However, for $M \neq 1$, the minimum current value happens at higher phase-shift angles.

An important observation is that the minimum $i_{Lk_{RMS}}$, for a given value of M , occurs at the same phase-shift angle, regardless of the power, and will depend only on M . This means that for any power, the minimum RMS current can be achieved by using variable switching frequency. This is an advantage, as it makes it possible to know the phase-shift angle at which the lowest value of $i_{Lk_{RMS}}$ occurs, only by knowing the voltages. This facilitates a possible control algorithm oriented to minimize conduction losses, in which the phase shift is set as a function of M to work with minimum $i_{Lk_{RMS}}$, and the frequency may be used to modulate the power transfer. Another observation is that the minimum $i_{Lk_{RMS}}$ is always inside the ZVS limit.

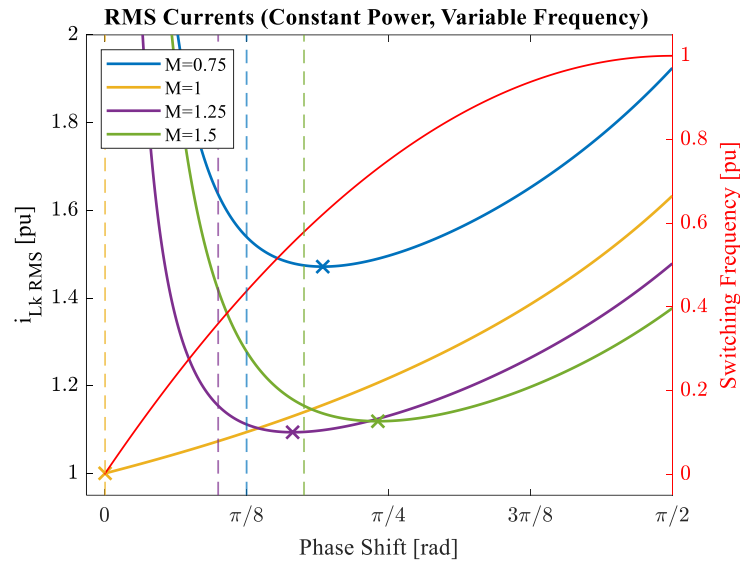


Figure 3. DAB converter normalized RMS currents (left y-axis) and normalized switching frequency (right y-axis), at different operating points: $M = 0.75$ (blue), $M = 1$ (yellow), $M = 1.25$ (purple), and $M = 1.5$ (green). Ideal ZVS limits are shown in vertical dashed lines in their respective operating point colors.

Reactive currents in the DAB converter are necessary for ZVS operation, as they provide the energy for soft-switching. During the dead time, the reactive currents flow through the body diode of the MOSFET. These currents need to be big enough to provide the energy to charge and discharge the parasitic capacitances of the MOSFETs and turn on the device with ZVS. The minimum currents needed for ZVS, i_{1min} and i_{2min} , can be defined as follows [10,31]:

$$i_{1min} \geq \sqrt{\frac{C_{oss,eq1} V_1^2}{L_{k1}}} \tag{7}$$

$$i_{2min} \geq \sqrt{\frac{C_{oss,eq2} V_2^2}{L_{k2}}}, \tag{8}$$

where $C_{oss,eq1}$ and $C_{oss,eq2}$ are the total parasitic capacitances at FB_1 and FB_2 , respectively. L_{k1} and L_{k2} represent the inductance L_k from Figure 1 referred to FB_1 and FB_2 , respectively. The currents i_{1min} and i_{2min} are also referred to their respective FBs. It is possible to estimate the MOSFET C_{oss} at a certain operating point [32,33]. However, for simplicity, in this analysis it is considered constant, and its value is approximated using the C_{oss} value given by the datasheet. These currents define the ZVS limits, which are discussed in the next subsection.

Figure 4 shows the normalized reactive currents for different values of M . The average reactive currents can be obtained from the shadowed area in Figure 2, and can be described as follows:

$$i_{q1} = \frac{f_s L_k i_1^2}{V_1 + V_2 n} \tag{9}$$

$$i_{q2} = \frac{f_s L_k i_2^2}{V_1 + V_2 n}, \tag{10}$$

where i_{q1} and i_{q2} correspond to the reactive current in FB_1 and FB_2 , respectively. The normalization is done using the average input current as the base value. The reactive currents in FB_1 and FB_2 are shown in blue and orange, respectively, while the ideal ZVS limits are marked with a vertical dashed line. It is evident that the reactive current becomes zero at the ZVS limit in its respective FB, as it can also be deduced from Figure 2. Both reactive currents are minimum at this point. Like the RMS currents, for $M = 1$, the reactive currents increase with the phase shift, and as M gets farther away from 1, the phase shift at

which they are at minimum increases. For $M = 1$, the currents in both FBs are equivalent. It can be concluded that operating the converter with phase-shift angles close to the ZVS limit will have the lower reactive current values. Note that Figure 4 shows reactive currents at the left of the ideal ZVS limit, however, they do not provide ZVS operation, as they flow through the device after it has been turned on.

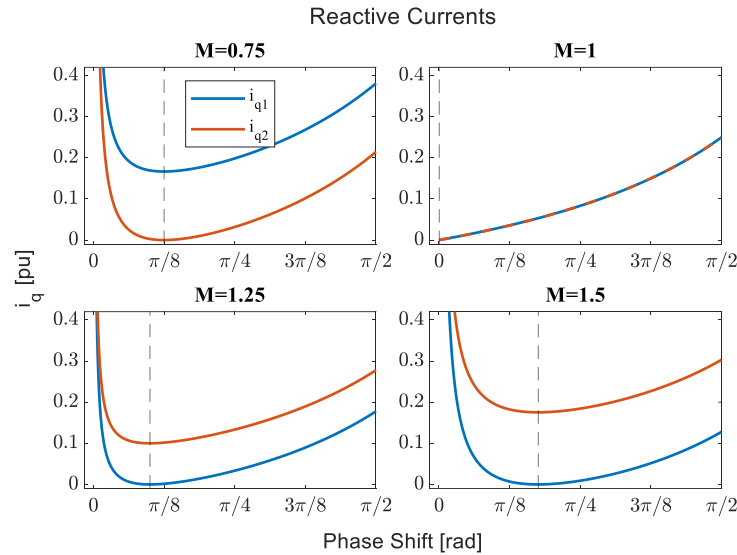


Figure 4. DAB converter normalized reactive currents in FB₁ (blue) and FB₂ (orange), for different operating points. The ideal ZVS limit is shown in vertical dashed line (black).

3.2. ZVS Boundaries

The limits for ZVS operation depend on the reactive current as mentioned previously. Considering the SPS modulation, and defining a minimum current that will provide the energy for the parasitic capacitances, it is evident that by using (5) and (6) to solve (2) and (3), the minimum angle that guarantees ZVS can be defined as below:

$$\varphi_{min} = \begin{cases} \frac{\pi(4f_s L_k (\frac{i_{1min}}{V_1}) + M - 1)}{2M}, & \text{for } M > 1 \\ \frac{\pi(4f_s L_k (\frac{i_{2min}}{V_1}) + 1 - M)}{2}, & \text{for } M < 1. \end{cases} \quad (11)$$

The effect of the parasitic capacitance modifies the ZVS limits as it can be seen from (5) and (6) [2]. The switching frequency as well as the voltages also affect the ZVS limits, as can be seen from (7). Figure 5 shows the modification of ZVS limits when f_s varies from 20 kHz (left) to 120 kHz (right). As it was previously highlighted, (11) stabilizes the minimum phase-shift to obtain ZVS. This value varies linearly with the switching frequency. Therefore, the higher f_s , the higher is the minimum phase shift. Hence, the ZVS limits the moves towards higher values of phase shift when f_s increases. The resulting phase shift can become significant enough to be non-negligible. Even so, if we consider the effect of the frequency when plotting the ZVS limits, every operating point will have its own ZVS limit. Therefore, for simplification purposes in presenting this analysis, these effects are neglected and the ZVS limits are considered ideal. This implies that the ZVS operation is true when $i_1 > 0$ and $i_2 > 0$. Thus, (7) can be simplified and rewritten as below:

$$\varphi_{min} = \begin{cases} \frac{\pi(M-1)}{2M}, & M > 1 \\ \frac{\pi(1-M)}{2}, & M < 1. \end{cases} \quad (12)$$

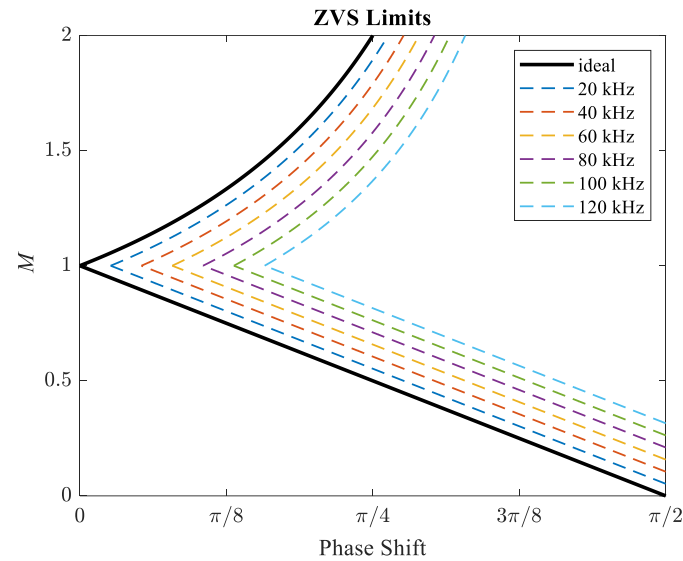


Figure 5. The influence of the switching frequency considering a variation from 20 kHz to 120 kHz. The ideal ZVS limits are shown in solid black line.

Note that now the ZVS limits are independent of the voltage values and depend only on their ratio, M . This simplification is beneficial for the converter design process, allowing the inclusion of other parameters at later design stages.

Having simplified the equations for calculating the ZVS limits, it is easier to plot different curves on the same plane using the ideal ZVS limits as a reference. To visualize the converter operation at different frequencies, it is useful to represent a constant power curve, ‘ M vs. phase shift’, as it provides insight into the relationship between the M and the ZVS limits. This curve can be obtained from (1) and it is described as follows:

$$M = \frac{V_2^2 n^2 \varphi (\pi - \varphi)}{2\pi^2 f_s L_k P_{const}}, \tag{13}$$

where P_{const} is the constant power. Note that the curve must be referred to one of the voltages, which is selected arbitrarily, as it determines the ‘slope’ of the curve. For this analysis, each value of V_2 will have its own curve and M will vary as a function of V_1 .

Figure 6 shows the converter operating at constant power, evaluated at two different switching frequencies. The power curves are presented for three different values of V_2 . Solid lines represent the converter working at an arbitrary switching frequency, f_n , and the dashed line curves represent it working at $2f_n$. The colored areas represent the variation of the voltage range V_1 for each power curve in its respective color. The voltages are normalized. The figure shows the power curves in red, blue, and green, for $V_2 = 0.75, 1,$ and 1.25 , respectively. The voltage V_1 ranges from 0.8 to 1. From this figure, the influence of the switching frequency regarding the converter operating points with respect to the ZVS limits is clearly appreciated, as at $2f_n$ the converter operates within the ZVS limits throughout the whole voltage range. That is not the case for the switching frequency f_n , as it can be seen that for $V_2 = 1.25$, the whole operation range is outside the ZVS limits, and for $V_2 = 0.75$, it partially operates within the limits. It is observed that as M grows farther away from 1, higher frequencies are needed to keep the converter operating within the ZVS limits.

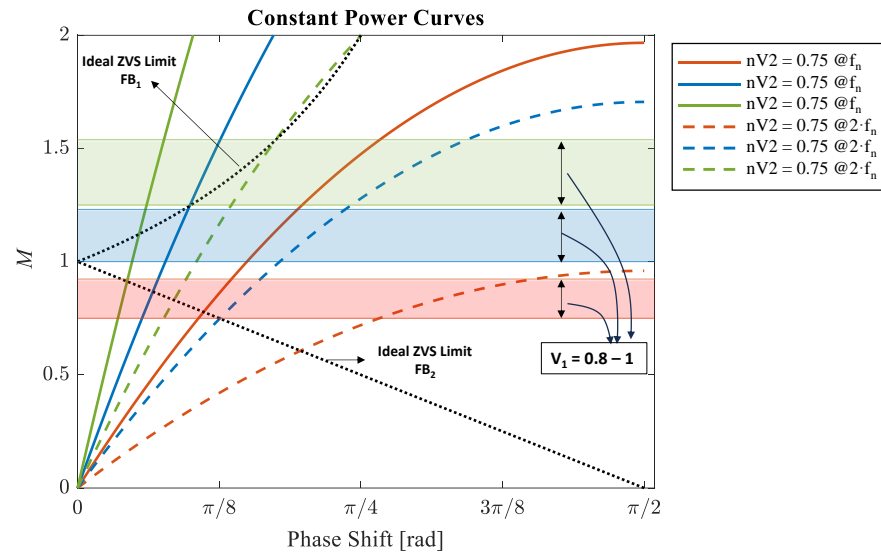


Figure 6. M vs phase shift constant power curves. Power curves are referred to V_2 values: 0.75 (red), 1 (blue) and 1.25 V (green). The colored areas represent the variation of V_1 from 0.8 to 1. Solid lines and dashed lines correspond to a switching frequency of f_n and $2 \cdot f_n$, respectively. The ideal ZVS limits are shown in black dotted lines.

3.3. Minimum Switching Frequency

When working at a certain power, the phase shift is a consequence of the given operating point, making it necessary to consider the switching frequency as a variable to modify the phase shift. This allows the power curve to move in any direction, making it possible to work at any given value of M without losing ZVS. According to the analysis presented in the previous subsection, it becomes necessary to define the minimum frequency needed to operate within the ZVS limits for any given operating point. From Figure 6, it is stated that higher frequencies are needed to move the power curves inside the ZVS limits. However, increasing the switching frequency too much may lead to higher conduction and switching losses. Therefore, it is beneficial to work at low phase-shift angles, close to the ZVS limits, where the RMS currents are low, as well as the switching frequency.

The minimum switching frequency needed to guarantee ZVS at any operating point can be found by evaluating the φ_{min} from (12) into (13) resulting in the following:

$$f_{s_{min}}(V_1, V_2) = \begin{cases} \frac{V_2^2 n^2 (M^2 - 1)}{8L_k P_{const} M^3}, & \text{for } M > 1 \\ \frac{V_2^2 n^2 (1 - M^2)}{8L_k P_{const} M}, & \text{for } M < 1, \end{cases} \quad (14)$$

noting that the equation must also be referred to one of the voltages, V_2 in this case. The minimum frequency for the entire range of operation can be found by substituting the variables V_2 and M with $V_{2_{max}}$ and M_{max} , respectively, for $M > 1$, and with $V_{2_{min}}$ and M_{min} , respectively, for $M < 1$.

Figure 7 shows three power curves at 10 kW referred to a voltage $V_2 = 500$ V. The curves have a switching frequency of 50 kHz (blue), 41 kHz (green), and 30 kHz (red). It is evident that by modifying the switching frequency, the converter is able also to modify the phase shift, and thus work with the minimum phase shift, staying within the ZVS operation limits. The switching frequency must be increased when the operating point is outside the ZVS limits (red operating point) and decreased to obtain lower reactive currents (blue operating point). The green operating point is on the ZVS limits, where it operates at the minimum switching frequency and minimum phase shift.

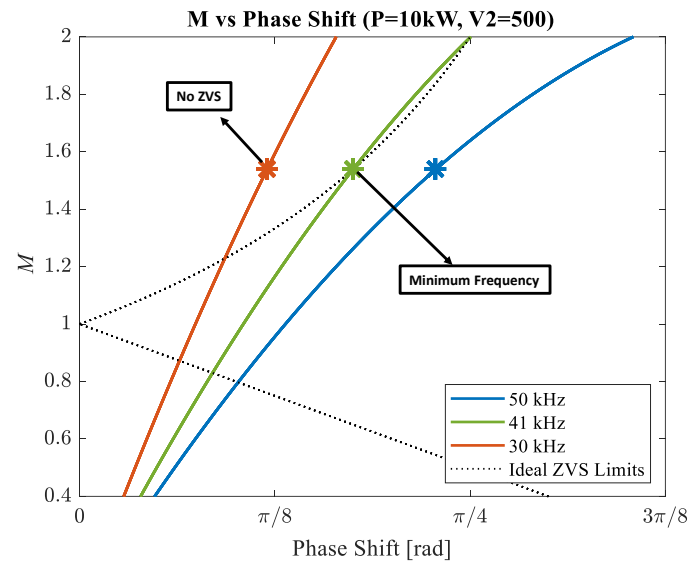


Figure 7. The converter curves operating at 10 kW, referred to $V_2 = 500$ V at $M = 1.5$, are shown at different switching frequencies: 50 kHz (blue), 41 kHz (green), 30 kHz (red). The ideal ZVS limits are shown in dashed black lines.

4. Experimental Results

This section contains two main objectives: to validate the theoretical analysis regarding the RMS currents and to assess the implementation of the switching frequency as a control variable to ensure ZVS operation over a wide voltage range. The validation process is performed with a DAB converter prototype shown in Figure 8, and whose characteristics are described in Table 1. The converter maximum power, at 20 kHz and maximum voltages, is 43 kW, although the switching devices are designed to operate at a nominal power of 20 kW. The tests and analysis are performed at a constant power of 10 kW. This value is selected to allow the converter to work throughout the voltage and frequency ranges, maintaining the operating points around the ZVS limits. The switching frequency, f_s , ranges from 20 kHz to 70 kHz. The input voltage, V_1 , ranges from 300 V to 500 V and the output voltage, V_2 , ranges from 650 V to 800 V.

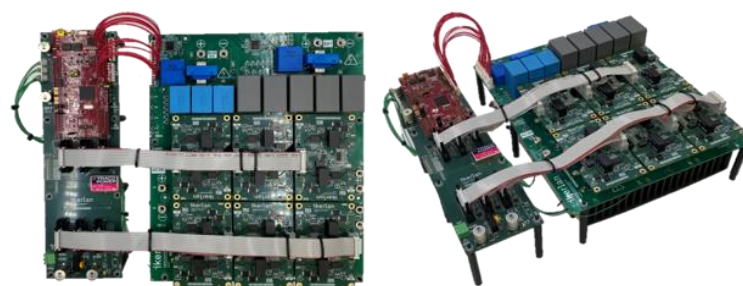


Figure 8. The DAB converter prototype.

Table 1. DAB converter parameters.

Parameter	Value
V_1 [V]	650–800
V_2 [V]	300–500
Lk [μ H]	114
P_n [kW]	10
f_s [kHz]	20–70
n	2
MOSFET	FF11MR12W1M1_B11

The converter is tested using two different bidirectional voltage sources connected to the converter ports. The switching devices are SiC MOSFETs on both FBs, and the transformer turns ratio is $n = 2$. The converter is controlled by a Microcontroller Unit (MCU), Texas LaunchPad F28379D.

Figure 9 shows the experimental validation of the theoretical $i_{Lk_{RMS}}$ normalized curves. The curves show the theoretical values, and the operation points from the experimental results are marked with 'x' in its respective color. The ideal ZVS limits are shown in dashed vertical lines for each value of M , in their respective color. Each operating point varies the phase shift along with the switching frequency to maintain a constant power of 10 kW. The results match the theoretical curves, validating the presented analysis regarding the RMS currents. The operating points in Figure 9, are described in Table 2, showing the voltages, the phase shift, the switching frequency, and the RMS current for each operating point. The table is sorted from smallest to largest phase shift for each value of M . The efficiencies shown in Table 2 are for reference, as the converter is not optimized, and there are several factors that may impact the power losses. The currents in Figure 9 are normalized as follows: $i_{Lk_{RMS}} [pu] = \frac{i_{Lk_{RMS}}}{\frac{P_H}{V_1}}$.

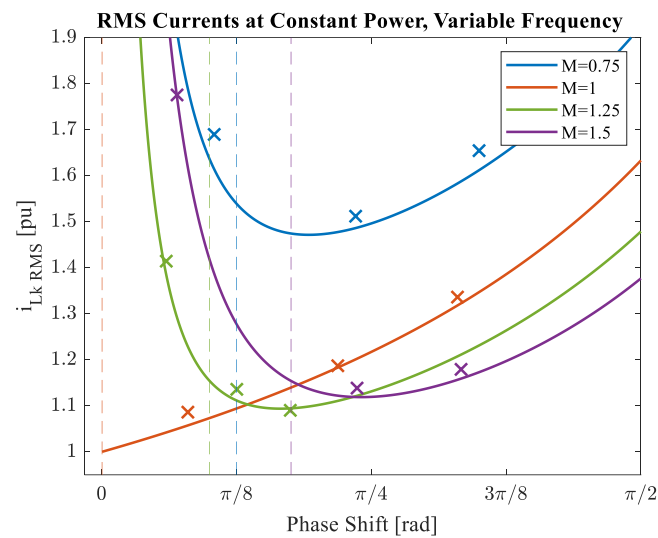


Figure 9. Experimental results. Normalized $i_{Lk_{RMS}}$ at different operating points at constant power of 10 kW and variable switching frequency. The operating points from the experimental results are marked with an 'x' in its respective color. The vertical dashed lines represent the ideal ZVS limits for each value of M in their respective color.

Table 2. Constant power operating points.

M	V ₁ [V]	V ₂ [V]	φ [rad]	f_s [kHz]	$i_{Lk_{RMS}}$ [A]	η [%]	Power [kW]
0.75	800	300	0.33	20	21.12	97.25	10.006
			0.74	38	18.9	96.86	10.012
			1.1	50	20.68	95.83	10.002
1	800	400	0.25	20	13.58	98.28	10.009
			0.69	50	14.84	96.60	10.002
	700	350	1.03	50	19.09	96.14	10.012
			0.19	20	17.68	95.54	10.032
1.25	800	500	0.39	38	14.2	94.21	10.016
			0.55	50	13.63	95.88	10.002
			0.22	20	26.63	93.99	9.999
1.54	650	500	0.74	51.5	17.08	94.55	10.000
			1.05	66.2	17.69	93.99	10.000

Figure 10 shows constant power curves for two different cases. Each case compares two different operating points. Figure 10a,c,e corresponds to the first case, operating at 10 kW, $V_1 = 750$ V, $V_2 = 500$ V, at two different switching frequencies: 20 kHz and 42.5 kHz. Figure 10a shows both operating points marked with an asterisk and their corresponding efficiencies. The first operating point switches at 20 kHz (blue) outside the ZVS limits, and the second switches at 42.5 kHz inside the ZVS limits. As expected, the operating point moves within the ZVS limits by increasing the switching frequency. Figure 10b,d,f shows the second case where the converter is operating at 10 kW, $V_1 = 800$ V, $V_2 = 300$ V, and at two different switching frequencies: 20 kHz and 38 kHz. Like the first case, Figure 10b shows both operating points marked with an asterisk and their corresponding efficiencies. The first operating point switches at 20 kHz (blue) outside the ZVS limits, and the second switches at 38 kHz inside the ZVS limits. In the same manner as the previous case, increasing the frequency allows the operating point to move within the ZVS limits. This can also be appreciated from the converter current waveforms. Figure 10c–f shows the following waveforms for 20 kHz, 42.5 kHz, 20 kHz, 38 kHz, respectively: the AC voltages v_1 , v_2 , the inductor current i_{Lk} , and the current values at the switching instant i_1 and i_2 . For both cases, it can be appreciated from the inductor current at the switching instant that for the lower frequencies, the value is negative, therefore it is not operating with ZVS. According to (3), the current value needs to be positive to be in ZVS operation. At higher frequencies, the value of the current at the switching instants becomes positive, implying the converter is soft-switching.

Figure 11a,c,e shows a case for $M = 1$, in which ZVS operation should apply throughout the whole operation range (considering ideal ZVS limits). The operating points are defined by $V_1 = 700$ V, $V_2 = 350$ V, at two different switching frequencies: 20 kHz and 50 kHz. In Figure 11a, both operating points are marked with an asterisk and their efficiency is shown in their respective colors. The following waveforms are shown in Figure 11c,e for 20 kHz and 50 kHz, respectively: the AC voltages v_1 , v_2 , the inductor current i_{Lk} , and the current values at the switching instant i_1 and i_2 . Both operating points in Figure 11a are within the limits as the current values i_1 and i_2 are both positive in Figure 11c,e.

Figure 11b,d,f shows the operation point at 10 kW, $V_1 = 800$ V, $V_2 = 500$ V. For this figure, the real ZVS limits are estimated for FB_1 using (7), where (5) is as follows:

$$i_{1min} \geq \sqrt{\frac{4C_{oss_{eq1}} V_1^2}{L_{k1}}} = 2.48\text{A}. \quad (15)$$

This operating point is analyzed with two different frequencies, 38 kHz (blue) and 48 kHz (green). The ZVS limits are shown for both frequencies in their respective colors. Figure 11d,f, shows the waveforms for the operating points switching at 38 and 48 kHz, respectively. It can be seen that both currents i_1 and i_2 are positive in both (d) and (f), however in (d), i_1 is approximately 2.5 A, while in (f) it is approximately 6 A. In (d), the value of i_1 is close to i_{min} , and the converter is operating at the ZVS limit, as can also be seen in (b), where the operating point of 38 kHz (blue) is at the ZVS limit. The efficiency measured at these operating points is 94.21% and 95.61% for 38 and 48 kHz, respectively. Regarding the ZVS limits, the minimum current needed for ZVS from (7) will be around the same (assuming constant C_{oss}), leaving the frequency as the main factor affecting them in a relevant way.

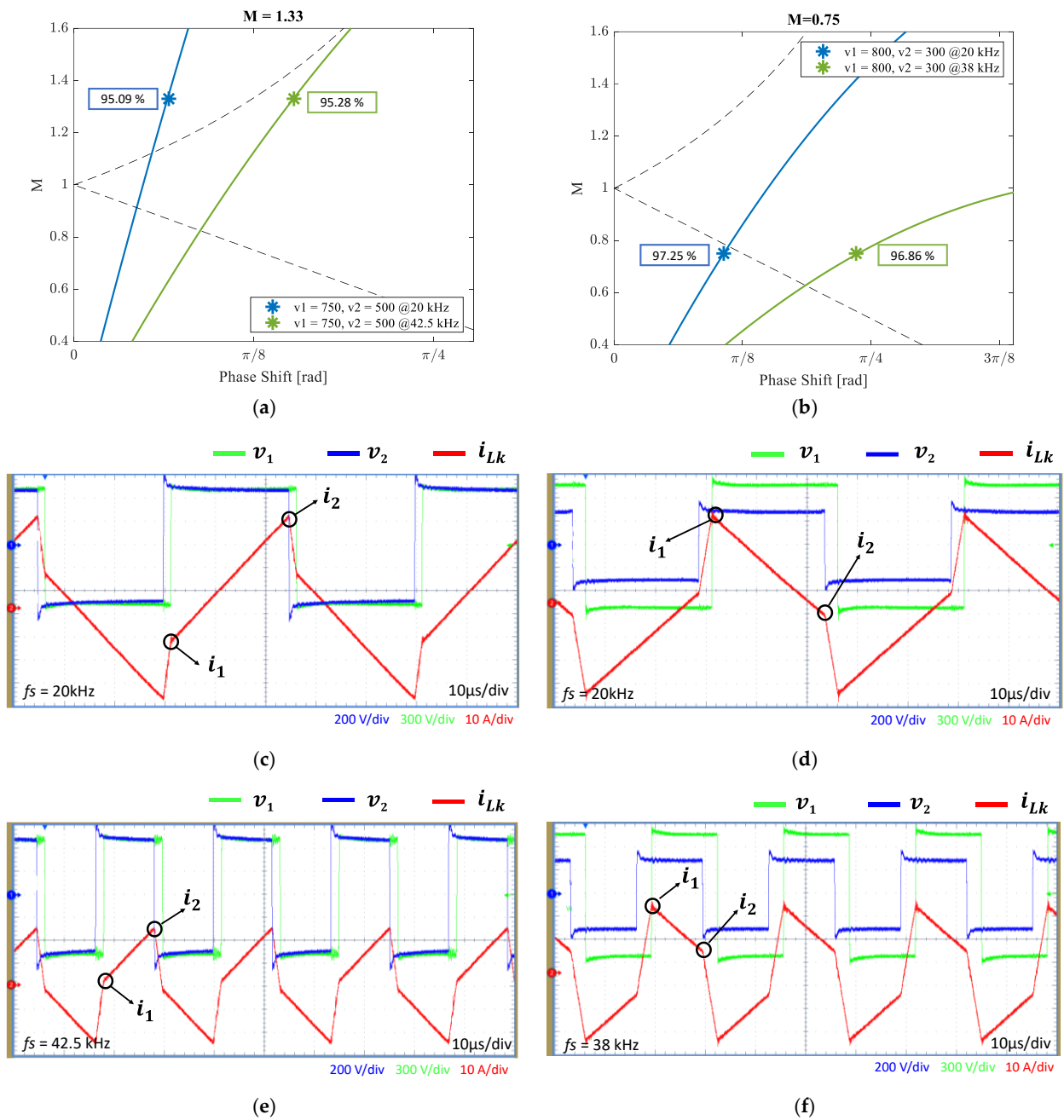


Figure 10. Converter operating at constant power and variable switching frequency at different operating points: (a) 20 kHz (blue) and 42.5 kHz (green); (b) 20 kHz (blue) and 38 kHz (green); (c) and (e) correspond to the operating point of (a) at 20 kHz and 42.5 kHz, respectively. (d,f) correspond to the operating point of (b) at 20 kHz and 38 kHz, respectively. (c–f) show the inductor current, i_{Lk} , in red. The current values at the switching instants are indicated in black as i_1 and i_2 and the voltages v_1 and v_2 are shown in green and blue, respectively.

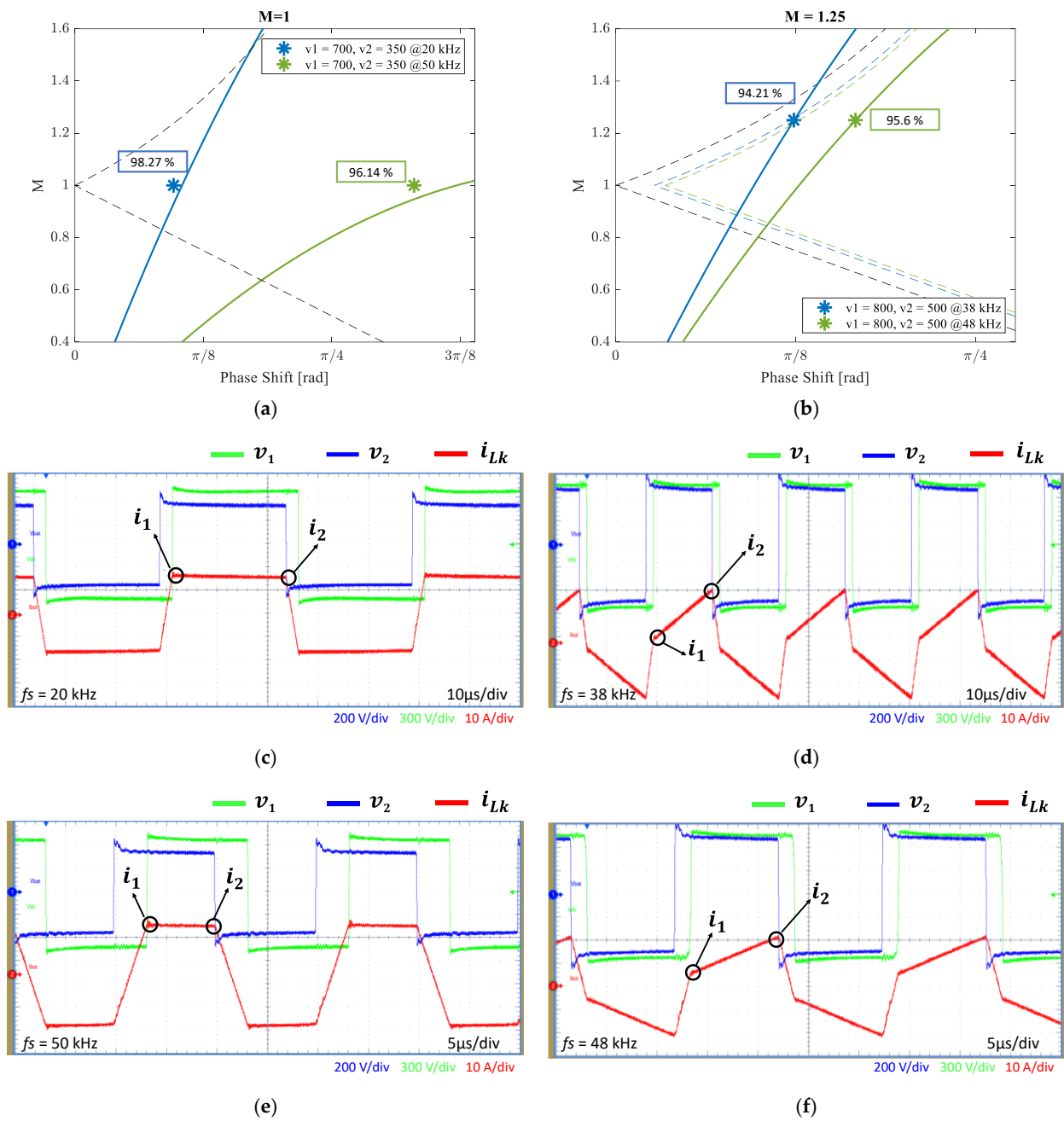


Figure 11. Converter operating at constant power and variable switching frequency at different operating points: (a) 20 kHz (blue) and 50 kHz (green); (b) 38 kHz (blue) and 48 kHz (green); (c,e) correspond to the operating point of (a) at 20 kHz and 50 kHz, respectively. (d,f) correspond to the operating point of (b) at 38 kHz and 48 kHz, respectively. (c–f), show the inductor current, i_{Lk} , in red. The current values at the switching instants are indicated in black as i_1 and i_2 and the voltages v_1 and v_2 are shown in green and blue, respectively.

5. Conclusions

This study analyzed the DAB converter, incorporating the switching frequency as an additional control variable. The influence of the switching frequency on the converter operating points is clearly presented, considering constant power operation. The RMS, reactive currents, and ZVS limits were analyzed, showing the impact of the switching frequency on them, as well as their dependance on M . Furthermore, a DAB prototype was used for validating the analysis.

In conclusion, implementing the switching frequency as a control variable provides an additional degree of freedom to the converter. It makes it possible to vary the phase shift while maintaining a constant power operation. This allows the converter to work within the ZVS limits at any operating point throughout a wide voltage range. Moreover, it provides the ability to reduce the RMS and reactive currents.

The study reveals that the minimum $i_{Lk_{RMS}}$, for a given value of M , occurs at a specific phase-shift angle, determined by M and independent of the power. Importantly, this value is always within the ideal ZVS limits. These findings offer valuable insights for both the converter design and the control algorithms.

Author Contributions: Conceptualization, A.C., A.F.-H., F.G.-H., A.V. and A.R.; methodology, A.C., A.F.-H., F.G.-H., A.V. and A.R.; software, A.C.; validation, A.C.; formal analysis, A.C.; investigation, A.C.; resources, A.F.-H. and F.G.-H.; data curation, A.C.; writing—original draft preparation, A.C.; writing—review and editing, A.C., A.F.-H., F.G.-H., A.V. and A.R.; visualization, A.C.; supervision, A.F.-H., F.G.-H., A.V. and A.R.; project administration, A.F.-H., F.G.-H., A.V. and A.R.; funding acquisition, A.F.-H., F.G.-H., A.V. and A.R. All authors have read and agreed to the published version of the manuscript.

Funding: This research was funded by the Principality of Asturias under the Severo Ochoa program, grant number PA-23-BP21-204, by FICYT under project SV-PA-21-AYUD/2021/51931, and by the AEI under the project MCINN-TED2021-130939B-I00.

Data Availability Statement: The data can be shared up on request.

Conflicts of Interest: The authors declare no conflicts of interest.

References

1. De Doncker, R.W.; Divan, D.M.; Kheraluwala, M.H. A Three-Phase Soft-Switched High Power Density DC/DC Converter for High Power Applications. *IEEE Ind. Appl. Soc. Annu. Meet.* **1988**, *1*, 796–805.
2. Kheraluwala, M.H.; Gascoigne, R.W.; Divan, D.M.; Baumann, E.D. Performance Characterization of a High-Power Dual Active Bridge dc-to-dc Converter. *IEEE Trans. Ind. Appl.* **1992**, *28*, 1294–1301. [[CrossRef](#)]
3. Schibli, N. *Symmetrical Multilevel Converters with Two Quadrant DC-DC Feeding*; École Polytechnique Fédérale de Lausanne: Lausanne, Switzerland, 2000.
4. Krismer, F. *Modeling and Optimization of Bidirectional Dual Active Bridge DC—DC Converter Topologies*; ETH Zurich: Zürich, Switzerland, 2010.
5. Rodríguez, A.; Vázquez, A.; Lamar, D.G.; Hernando, M.M.; Sebastián, J. Different purpose design strategies and techniques to improve the performance of a dual active bridge with phase-shift control. *IEEE Trans. Power Electron.* **2015**, *30*, 790–804. [[CrossRef](#)]
6. Dong, J.; Pou, J.; Li, X.; Mukherjee, S.; Gupta, A.K.; Zeng, Y. Hybrid Duty Ratio Phase-Shift Modulation for a Si + SiC Neutral-Point-Clamped Dual-Active-Bridge Converter. *IEEE Access* **2023**, *11*, 129866–129881. [[CrossRef](#)]
7. Zhao, B.; Song, Q.; Liu, W. Power characterization of isolated bidirectional dual-active-bridge dc-dc converter with dual-phase-shift control. *IEEE Trans. Power Electron.* **2012**, *27*, 4172–4176. [[CrossRef](#)]
8. Gu, H.; Jiang, D.; Yin, R.; Huang, S.; Liang, Y.; Wang, Y. Power characteristics analysis of bidirectional full-bridge DC-DC converter with triple-phase-shift control. In Proceedings of the 2015 10th IEEE Conference on Industrial Electronics and Applications, ICIEA 2015, Auckland, New Zealand, 5–17 June 2015; pp. 363–368. [[CrossRef](#)]
9. Zeng, Y.; Pou, J.; Sun, C.; Mukherjee, S.; Xu, X.; Gupta, A.K.; Dong, J. Autonomous Input Voltage Sharing Control and Triple Phase Shift Modulation Method for ISOP-DAB Converter in DC Microgrid: A Multiagent Deep Reinforcement Learning-Based Method. *IEEE Trans. Power Electron.* **2023**, *38*, 2985–3000. [[CrossRef](#)]
10. Yan, Y.; Bai, H.; Foote, A.; Wang, W. Securing Full-Power-Range Zero-Voltage Switching in Both Steady-State and Transient Operations for a Dual-Active-Bridge-Based Bidirectional Electric Vehicle Charger. *IEEE Trans. Power Electron.* **2020**, *35*, 7506–7519. [[CrossRef](#)]
11. Fernandez-Hernandez, A.; Gonzalez-Hernando, F.; Garcia-Bediaga, A.; Villar, I.; Abad, G. Design Space Analysis of the Dual-Active-Bridge Converter for More Electric Aircraft. *Energies* **2022**, *15*, 9503. [[CrossRef](#)]
12. Krismer, F.; Kolar, J.W. Closed form solution for minimum conduction loss modulation of DAB converters. *IEEE Trans. Power Electron.* **2012**, *27*, 174–188. [[CrossRef](#)]
13. Xie, H.; Zhang, Y.; Cai, F. Variable inductance control of DAB converter to reduce reactive power. In Proceedings of the 2023 IEEE 6th International Electrical and Energy Conference, CIEEC 2023, Hefei, China, 2–14 May 2023; Institute of Electrical and Electronics Engineers Inc.: Piscataway, NJ, USA, 2023; pp. 1360–1364. [[CrossRef](#)]

14. Saeed, S.; Garcia, J. Extended Operational Range of Dual-Active-Bridge Converters by using Variable Magnetic Devices. In Proceedings of the 2019 IEEE Applied Power Electronics Conference and Exposition (APEC), Anaheim, CA, USA, 17–21 March 2019. [\[CrossRef\]](#)
15. Yin, Y.; Wang, W.; Wang, N.; Chen, A. An Online Efficiency Optimization Strategy Based on Variable-Frequency Phase-Shift Modulation for Dual-Active-Bridge Converters. In Proceedings of the 2023 11th International Conference on Power Electronics and ECCE Asia (ICPE 2023—ECCE Asia), Jeju, Republic of Korea, 22–25 May 2023. [\[CrossRef\]](#)
16. Guidi, G.; Pavlovsky, M.; Kawamura, A.; Imakubo, T.; Sasaki, Y. Improvement of Light Load Efficiency of Dual Active Bridge DC-DC Converter by Using Dual Leakage Transformer and Variable Frequency. In Proceedings of the 2010 IEEE Energy Conversion Congress and Exposition, Atlanta, GA, USA, 12–16 September 2010. [\[CrossRef\]](#)
17. Cárcamo, A.; Vázquez, A.; Rodríguez, A.; Lamar, D.G.; Hernando, M.M.; Gómez, A.A.; Remón, D. Control Strategy for DAB using SPS for Integration of Modular Batteries in EV. In Proceedings of the 2023 25th European Conference on Power Electronics and Applications (EPE'23 ECCE Europe), Aalborg, Denmark, 4–8 September 2023. [\[CrossRef\]](#)
18. Everts, J.; Krismer, F.; Van Den Keybus, J.; Driesen, J.; Kolar, J.W. Optimal zvs modulation of single-phase single-stage bidirectional dab ac-dc converters. *IEEE Trans. Power Electron.* **2014**, *29*, 3954–3970. [\[CrossRef\]](#)
19. Esteve, V.; Bellido, J.L.; Jordán, J.; Dede, E.J. Improving the Efficiency of an Isolated Bidirectional Dual Active Bridge DC–DC Converter Using Variable Frequency. *Electronics* **2024**, *13*, 294. [\[CrossRef\]](#)
20. Saegmueller, M.; Hackl, C.; Witzmann, R.; Richter, R. Analytic Solutions for Minimum Conduction Loss Modulation of Dual Active Bridge Converters Including Frequency Variation. In Proceedings of the IECON 2020 The 46th Annual Conference of the IEEE Industrial Electronics Society, Singapore, 18–21 October 2020. [\[CrossRef\]](#)
21. Erni, I.R.; Vidal-Idiarte, E.; Calvente, J.; Guasch-Pesquer, L. Small Signal Modelling for Variable Frequency Control with Maximum Efficiency Point Tracking of DAB Converter. *IEEE Access* **2021**, *9*, 85289–85299. [\[CrossRef\]](#)
22. Hiltunen, J.; Vaisanen, V.; Juntunen, R.; Silventoinen, P. Variable-Frequency Phase Shift Modulation of a Dual Active Bridge Converter. *IEEE Trans. Power Electron.* **2015**, *30*, 7138–7148. [\[CrossRef\]](#)
23. Mandal, S.; Shukla, A.; Doolla, S. Optimizing Transformer RMS Current Using Single Phase Shift Variable Frequency Modulation for Dual Active Bridge DC-DC Converter. In Proceedings of the 2022 IEEE Energy Conversion Congress and Exposition, ECCE 2022, Detroit, MI, USA, 9–13 October 2022; Institute of Electrical and Electronics Engineers Inc.: Piscataway, NJ, USA, 2022. [\[CrossRef\]](#)
24. Ma, P.; Sha, D.; Zhang, D. High-Efficiency and Full Range ZVS Single-Stage Semi-DAB AC-DC Converter with Improved Modulation and Variable Frequency Control. *IEEE Trans. Power Electron.* **2024**, *39*, 6003–6016. [\[CrossRef\]](#)
25. Kazemtarghi, A.; Dey, S.; Mallik, A.; Johnson, N.G. Asymmetric Half-Frequency Modulation in DAB to Optimize the Conduction and Switching Losses in EV Charging Applications. *IEEE Trans. Transp. Electrif.* **2023**, *9*, 4196–4210. [\[CrossRef\]](#)
26. Zhao, X.; Jiang, D.; Chen, J.; Wang, Z.; Liu, Z. The Impact of Periodic Variable Switching Frequency Modulation on Power Transmission in Dual-Active-Bridge Converter and an Improved Scheme. *IEEE Trans. Power Electron.* **2023**, *38*, 13966–13976. [\[CrossRef\]](#)
27. Lyu, D.; Straathof, C.; Soeiro, T.B.; Qin, Z.; Bauer, P. ZVS-Optimized Constant and Variable Switching Frequency Modulation Schemes for Dual Active Bridge Converters. *IEEE Open J. Power Electron.* **2023**, *4*, 801–816. [\[CrossRef\]](#)
28. Fan, Z.; Lu, H.; Chai, J.; Li, Y.; Sun, X. Partition Variable Frequency and EPS Hybrid Control to Achieve Full Load Range ZVS for Dual Active Bridge Converters. *IEEE J. Emerg. Sel. Top. Power Electron.* **2024**, *12*, 143–155. [\[CrossRef\]](#)
29. Tang, Y.; Hu, W.; Cao, D.; Hou, N.; Li, Z.; Li, Y.W.; Chen, Z.; Blaabjerg, F. Deep Reinforcement Learning Aided Variable-Frequency Triple-Phase-Shift Control for Dual-Active-Bridge Converter. *IEEE Trans. Ind. Electron.* **2023**, *70*, 10506–10515. [\[CrossRef\]](#)
30. Fernandez-Hernandez, A.; Garcia-Bediaga, A.; Villar, I.; Abad, G. Analytical equations of the currents in dual active bridge converter for more electric aircraft. In Proceedings of the 2020 IEEE Vehicle Power and Propulsion Conference, VPPC 2020—Proceedings, Virtual Conference, 18 November–16 December 2020; Institute of Electrical and Electronics Engineers Inc.: Piscataway, NJ, USA, 2020. [\[CrossRef\]](#)
31. Li, S.; Yuan, X.; Wang, Z.; Wang, K.; Zhang, Y.; Wu, X. A Unified Optimal Modulation Strategy for DAB Converters to Trade-off the Backflow Power Reduction and All ZVS in the Full Operating Range. *IEEE J. Emerg. Sel. Top. Power Electron.* **2023**, *11*, 5701–5723. [\[CrossRef\]](#)
32. Costinett, D.; Maksimovic, D.; Zane, R. Circuit-oriented treatment of nonlinear capacitances in switched-mode power supplies. *IEEE Trans. Power Electron.* **2015**, *30*, 985–995. [\[CrossRef\]](#)
33. Kasper, M.; Burkart, R.M.; Deboy, G.; Kolar, J.W. ZVS of Power MOSFETs Revisited. *IEEE Trans. Power Electron.* **2016**, *31*, 8063–8067. [\[CrossRef\]](#)

Disclaimer/Publisher's Note: The statements, opinions and data contained in all publications are solely those of the individual author(s) and contributor(s) and not of MDPI and/or the editor(s). MDPI and/or the editor(s) disclaim responsibility for any injury to people or property resulting from any ideas, methods, instructions or products referred to in the content.